Energy Nexus 7 (2022) 100114

Contents lists available at ScienceDirect

Energy Nexus

journal homepage: www.elsevier.com/locate/nexus

# Utilization of Excess Steam from a Vent Valve in a Geothermal Power Plant

Putri Sundari[a], Prihadi Setyo Darmanto[b], Bayu Rudiyanto[c,*], Miftah Hijriawan[d]

[a] Departement of Mechanical Engineering, Faculty of Engineering, Universitas Gresik, Jl. Arif Rahman Hakim Gresik No.2B, Kramatandap, Gresik 61111, Indonesia
[b] Faculty of Mechanical and Aerospace Engineering, Institut Teknologi Bandung, Jl. Ganesha 10. Bandung 40132, Indonesia
[c] Energy Engineering Laboratory, Departement of Renewable Energy Engineering, Politeknik Negeri, Jember, Jl. Mastrip 164, Jember 68121, Indonesia
[d] Graduate Program of Mechanical Engineering, Universitas Sebelas Maret, Jl. Ir. Sutami 36, Surakarta 57126, Indonesia

ARTICLE INFO

*Keywords:*
Dry-steam cycle
Binary cycle
Kalina cycle
Excess steam
LEGC
Capacity factor

ABSTRACT

A novel strategy is presented for the utilization of the excess steam released into the atmosphere from the vent valve of a geothermal power plant. In particular, three possible approaches are considered: dry-steam cycle, binary cycle, and Kalina cycle. Thermodynamic models of these different power cycles are defined accordingly. The simulations are carried out using Aspen HYSYS®, used to solve the corresponding mass and energy balance equations. The feasibility and advantages of the different approaches are discussed from different points of view, i.e., energy, net power, and overall efficiency. Moreover, exergy analysis is used to identify the location, magnitude, and origin of thermodynamic inefficiencies. Economic aspects are also considered in terms of electricity or levelized electricity generating cost (LEGC) for the three considered cycles. Performances are quantified in terms of Capacity Factor (CF), the ratio between the actual power produced by the generator in a given period and the maximum output power that can be achieved according to the design capacity. The environmental impact is also considered.

## Introduction

Geothermal energy is a type of renewable energy which is derived steam vapor within the sub-surface of the earth and can be transformed into electricity. The conversion of geothermal energy into electrical energy is neither a cheap nor a simple process. Therefore there is a real need to use the available energy efficiently [1–3]. By far, there are three different types of geothermal power plants which are (1) the flash cycle, (2) the dry-steam cycle, and (3) the binary-Kalina cycle [4].

Compared with other geothermal cycles, the dry-steam cycle is relatively simple with a less complicated component so that the cost can be lower than other cycles [5]. Furthermore, the dry-steam cycle contains more thermal energy due to the rich vapor condition of the steam, and it results in higher electricity production [6]. However, geothermal with dry-steam is very limited, estimated at 5% of all hydrothermal systems with temperatures above 200°C [7]. Therefore, improvement of the currently operating dry-steam cycle is necessary for sustainable electricity generation [8].

Some literature reported that the operating dry-steam cycle potentially causes significant losses due to excess steam release in the vent valve component [9,10]. The dry-steam from the production well in the geothermal power plant is received by a steam receiving header (SRH), equipped with an exhaust valve, before entering into the generating unit to control the incoming pressure within 6.5 bars, under the flow rate needed. Meanwhile, the mechanism involves controlling the valve that functions at all times to remove the excess steam into the environment due to the contract Steam Purchase Agreement. The 10% surplus of supplies aims to compensate for the load of electricity fluctuations in the interconnection network.

Other issues that should be discussed include plant sustainability because of the condition of the geothermal reservoir, which has depreciated over the operating period of more than 30 years. Suryadarma et al. reported a decrease in the temperature of 19°C (0.7°C/year), from the initial 245°C, the pressure drops from 34 to 9.3 bar, and the steam flow rate diminishes up to 3% per year [11]. This situation, therefore, requires that maximum utility of existing steam is a strategic road map to ensure sustainability in futuristic electricity production.

Several studies have focused on applying the excess steam from the vent valve in smaller-scale geothermal power plants. Prananto et al. researched by utilizing steam from the vent as a supply for the dry-steam cycle, using a variation of the gas removal system (GRS) to generate 15.94 MW of additional electricity [10]. Furthermore, Pratama also designed and simulated the operation of the Kalina cycle by utilizing the exhaust steam from the vent valve, producing optimal power by up to 4,251.72 kW, with an Ammonia mass fraction of 84% and pressure of 35 bars [12]. However, in previous research, the use of excess steam as a geothermal power plant only focused on how much power is generated

* Corresponding author.
*E-mail address:* bayu_rudianto@polije.ac.id (B. Rudiyanto).

https://doi.org/10.1016/j.nexus.2022.100114
Received 11 April 2022; Received in revised form 24 June 2022; Accepted 6 July 2022
Available online 15 July 2022

**Nomenclature**

| | |
|---|---|
| $c$ | specific heat capacity (J/kg.K) |
| $e$ | specific exergy (kJ/kg) |
| $\dot{E}$ | exergy flow (kJ |
| $h$ | enthalpy (kJ/kg) |
| $I$ | irreversibility (kW) |
| $\dot{m}$ | mass flow rate (kg/s) |
| η | efficiency (%) |
| $N$ | NCG fraction (%) |
| $P$ | pressure (bar) |
| $s$ | entropy (kJ/kg.K) |
| $T$ | temperature (°C) |
| $\Delta T_{pp}$ | pinch point temperature (°C) |
| $W$ | power/work (kW) |
| $y$ | exergy destruction ratio |

*Abbreviation*

| | |
|---|---|
| CATT | computer-aided thermodynamic table |
| CF | capacity factor |
| FCI | fixed capital investment |
| GRS | gas removal system |
| LEGC | levelized electricity generating cost |
| LMTD | log mean temperature difference |
| LRVP | liquid ring vacuum pump |
| MCWP | main cooling water pump |
| NCG | non condensable gas |
| ORC | organic rankine cycle |
| PEC | purchased equipment cost |
| REFPROP | reference fluid thermodynamic and transport properties |
| SRH | steam receiving header |
| TCC | total capital cost |
| TCI | total capital investment |
| TIP | turbine inlet pressure |

by a cycle designed based on energy analysis (1st Law of Thermodynamics) without considering the exact losses that would occur in a system.

Exergy analysis can be used to complete and optimize the thermal cycle analysis. This method will obtain an accurate analysis of the type, cause, and location of losses so that improvements can be made to get an optimal cycle design. Besides that, the performance of geothermal power plants and economic aspects are an absolute prerequisite to be evaluated in planning a power plant project, followed by environmental factors that must be considered along with the issue of global warming [1,13–16].

Furthermore, this research analyzes the utilization of excess steam for smaller-scale geothermal power plants using three different cycles, namely the dry-steam cycle, the binary cycle, and the Kalina cycle. The analysis will be carried out based on four criteria that are prerequisites for the feasibility of a power plant, including thermodynamic analysis to know which cycle is the most efficient and produces the greatest power, analysis of plant performance that can be known by the value of Capacity Factor (CF), economic analysis by comparing Levelized Electricity Generating Cost (LEGC) generated from each cycle, as well as an analysis of the environmental impacts of plant operations.

## Cycle Modeling in Geothermal Power Plants

Aspen HYSYS® carried out the simulation to modeling three different geothermal power plants and obtained the state properties corresponding with mass and energy balance. Furthermore, the data required was taken directly from the 24-h Log Operation History in the dry-steam power plant control room. This data also consists of assumptions based on the manual book in Engineering Department, as shown in Table 1. In this study, we assumed no heat loss from the heat exchanger utilities to the environment. Moreover, the potential and kinetic energy were neglected.

### *Dry-steam Cycle Modeling*

The model configuration of the dry-steam cycle was designed with the same components used currently in the observed Geothermal Power Plant, consisting of a demister, steam turbine, generator, condenser, gas removal system, and a cooling tower, as shown in Fig. 1. The demister served as a filter to ensure the dryness of steam entering the turbine. This cycle involved a gas removal system, in the form of a liquid ring vacuum pump (LRVP), with a target to produce a turbine power greater than the steam ejector [10].

Furthermore, the condenser used was a direct contact type with higher efficiency and physically smaller when compared with others [17]. Meanwhile, its pressure was assumed at 0.13 bar, which is still in the safe range for operation (0.06-0.15 bars). Conversely, the mechanical induced draft type tower equipment utilized the incoming airflow, assisted by a fan for cooling, and the highest air temperature from the average values in the geothermal power plant area (20°C) was applied in the model to obtain the appropriate cooling tower capacity. There are, however, 13 conditions in the dry-steam cycle, and each level is listed in Table 2. The mass, energy, and exergy balance equations used in the Aspen HYSYS® simulation report are shown in Table 3.

### *Binary Cycle Modeling*

In this model, the binary cycle as shown in Fig. 2, commonly called the Organic Rankine Cycle (ORC), involves the use of Isobutene as its working fluid (i-$C_4H_{10}$). This was chosen due to its critical temperature, which was lower than the value recorded for excess steam, where the maximum turbine intake pressure is obtained. Furthermore, the operating principle is similar to the Rankine cycle, consisting of fluid compression, liquid phase change into steam, expansion process to produce power, and conversion from steam to liquid, which occurs in a condenser. Therefore, the main equipment of this cycle includes the preheater, evaporator, turbine, condenser, pump, and the recuperator, which was added to utilize the residual steam, observed to possess sufficiently high energy (superheat phase) levels, capable of heating the working fluid before entering the preheater [18]. The mass, energy, and exergy balance equations used in the Aspen HYSYS® simulation report are shown in Table 4.

The initial parameters known as shown in Table 5 are the conditions of geothermal steam (point a), which encompasses the heat exchanger inlet, at a temperature of 160°C, obtained from the exhaust valve, and the heat exchanger (point c), at 70°C and above. This was chosen as the minimum because it is considered safe in instances where silica contained in the fluid has not solidified (the scaling process) [19,20]. The energy conversion occurring in each preheater and evaporator was analyzed using Eqs. (1) and (2) as follows:

$$\dot{m}_b c_b \left(T_b - T_c\right) = \dot{m}_{wf} \left(h_3 - h_2\right) \tag{1}$$

$$\dot{m}_b c_b \left(T_a - T_b\right) = \dot{m}_{wf} \left(h_4 - h_3\right) \tag{2}$$

$\dot{m}_b$ and $\dot{m}_{wf}$ represent the mass flow rate of the geothermal and organic working fluids, respectively $T_a$ is the temperature at which it enters the heat exchanger, which is always known at the initiation of the calculation. Furthermore, $\Delta T_{pp}$ was derived from the equipment specifications, illustrating that $T_b$ is known from the value $T_3 + \Delta T_{pp}$.

### *Kalina Cycle Modeling*

The components and principles applied in the Kalina cycle are similar to the binary type, as shown in Fig. 3. However, differences were

**Table 1**
Parameter data on Kamojang geothermal power plant.

| Parameter | Value | Unit | Parameter | Value | Unit |
|---|---|---|---|---|---|
| Steam mass flow rate | 27 | kg/s | Pressure drop demister | 0.3 | Bar |
| Pressure | 6.5 | Bar | Turbine Efficiency | 85 | % |
| Temperature | 162 | ˚C | Generator Efficiency | 95 | % |
| NCG levels (%) | 0.5 | % | Fan efficiency | 70 | % |
| Air temperature | 17-20 | ˚C | MCWP efficiency | 80 | % |
| Air pressure | 0.85 | Bar | Pump Efficiency | 80 | % |
| Humidity | 80 | % | Cooling water temperature | 27 | ˚C |

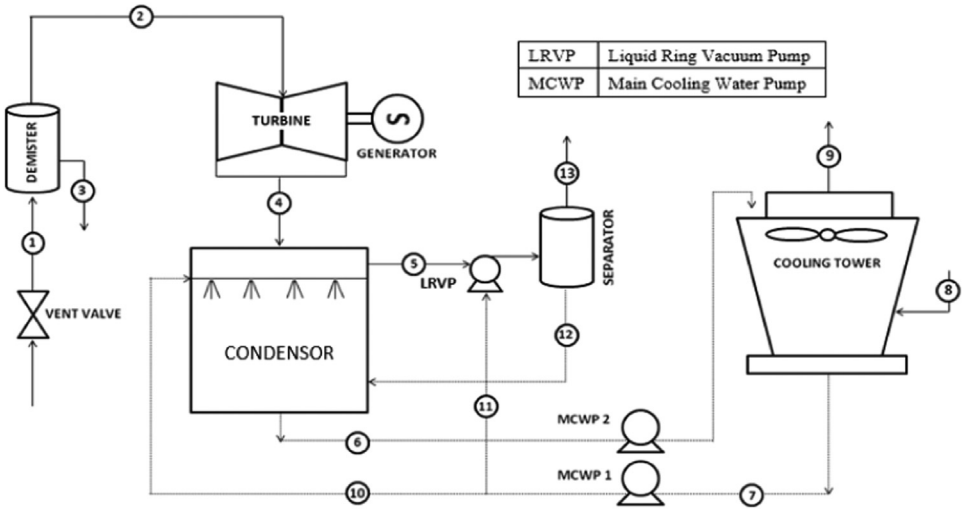


**Fig. 1.** Schematic diagram of the designed dry-steam cycle.

**Table 2**
The condition level for each dry-steam cycle.

| Condition | Information | ṁ (kg/s) | T (˚C) | P (bar) |
|---|---|---|---|---|
| 1 | Steam from the vent valve | 27 | 162.13 | 6.5 |
| 2 | Saturates steam enters the turbine | 26.91 | 160.26 | 6.2 |
| 3 | Discharged brine to blow down | 0.09 | 160.14 | 6.18 |
| 4 | Turbine exhaust steam | 26.91 | 51.18 | 0.13 |
| 5 | NCG enters LRVP | 0.134 | 51.18 | 0.13 |
| 6 | Condensate water of the condenser | 627.79 | 49 | 2.1 |
| 7 | Cooling water from the cooling tower | 601.1 | 27 | 0.85 |
| 8 | Cooling air enters the cooling tower | 506.28 | 20 | 0.85 |
| 9 | Saturated air discharged to environment | 506.28 | 34 | 0.8512 |
| 10 | Cooling water enters the condenser | 600.71 | 27 | 0.85 |
| 11 | Water enters LRVP | 0.3 | 27 | 0.85 |
| 12 | Water from LRVP enters the condenser | 0.3 | 29 | 0.85 |
| 13 | The remaining NCG discharged to the environment | 0.134 | 37 | 0.85 |

**Table 3**
The mass, energy, and exergy balance of the dry-steam cycle.

| Component | Mass Balance | Energy Balance | Exergy Balance |
|---|---|---|---|
| Demister | $\dot{m}_1 = \dot{m}_2 + \dot{m}_3$ | $\dot{m}_1 h_1 = \dot{m}_2 h_2 + \dot{m}_3 h_3$ | $\dot{m}_1 e_1 = \dot{m}_2 e_2 + \dot{m}_3 e_3 + I_{Demister}$ |
| Turbine | $\dot{m}_4 = \dot{m}_2$ | $\dot{m}_2 h_2 = W_T + \dot{m}_4 h_4$ | $\dot{m}_2 e_2 = W_T + \dot{m}_4 e_4 + I_{Turbine}$ |
| Condenser | $\dot{m}_4 + \dot{m}_{10} + \dot{m}_{12} = \dot{m}_5 + \dot{m}_6$ | $\dot{m}_4 h_4 + \dot{m}_{10} h_{10} + \dot{m}_{12} h_{12} = \dot{m}_5 h_5 + \dot{m}_6 h_6$ | $\dot{m}_4 e_4 + \dot{m}_{10} e_{10} + \dot{m}_{12} e_{12} = \dot{m}_5 e_5 + \dot{m}_6 e_6 + I_{Condenser}$ |

**Table 4**
The mass, energy, and exergy balance of the binary cycle.

| Component | Mass Balance | Energy Balance | Exergy Balance |
|---|---|---|---|
| Preheater | $\dot{m}_2 = \dot{m}_3,\ \dot{m}_b = \dot{m}_c$ | $\dot{m}_g(h_b - h_c) = \dot{m}_{wf}(h_3 - h_2)$ | $\dot{m}_b e_b + \dot{m}_3 e_3 = \dot{m}_c e_c + \dot{m}_2 e_2 + I_{Preheater}$ |
| Evaporator | $\dot{m}_3 = \dot{m}_4,\ \dot{m}_a = \dot{m}_b$ | $\dot{m}_g(h_a - h_b) = \dot{m}_{wf}(h_4 - h_3)$ | $\dot{m}_a e_a + \dot{m}_4 e_4 = \dot{m}_b e_b + \dot{m}_3 e_3 + I_{Evaporator}$ |
| Turbine | $\dot{m}_4 = \dot{m}_5$ | $\dot{m}_4 h_4 = W_T + \dot{m}_5 h_5$ | $\dot{m}_4 e_4 = W_T + \dot{m}_5 e_5 + I_{Turbine}$ |
| Condenser | $\dot{m}_6 = \dot{m}_7,\ \dot{m}_8 = \dot{m}_9$ | $\dot{m}_{wf}(h_6 - h_7) = \dot{m}_{ap}(h_9 - h_8)$ | $\dot{m}_6 e_6 + \dot{m}_9 e_9 = \dot{m}_7 e_7 + \dot{m}_8 e_8 + I_{Condenser}$ |
| Pump | $\dot{m}_7 = \dot{m}_1$ | $\dot{m}_1 h_1 = W_P + \dot{m}_7 h_7$ | $\dot{m}_1 e_1 = W_P + \dot{m}_7 e_7 - I_{Pump}$ |
| Recuperator | $\dot{m}_5 = \dot{m}_6,\ \dot{m}_1 = \dot{m}_2$ | $\dot{m}_5 h_5 + \dot{m}_1 h_1 = \dot{m}_6 h_6 + \dot{m}_2 h_2$ | $\dot{m}_5 e_5 + \dot{m}_1 e_1 = \dot{m}_6 e_6 + \dot{m}_2 e_2 + I_{Recuperator}$ |

**Table 5**
The state-level of each binary cycle condition.

| Condition | Information | ṁ (kg/s) | T (°C) | P (bar) |
|---|---|---|---|---|
| a | Geothermal fluids enter the evaporator | 27 | 160 | 6.175 |
| b | Geothermal fluid exits the evaporator | 27 | 160 | 6.175 |
| c | Geothermal fluid exits the preheater | 27 | 160 | 6.175 |
| 1 | Working fluid presses into the recuperator | 133.3 | 46.5 | 31.48 |
| 2 | The working fluid enters the preheater | 133.3 | 54 | 31.48 |
| 3 | The saturated working fluid enters the evaporator | 133.3 | 125.9 | 31.48 |
| 4 | Working fluid saturated steam enters the turbine | 133.3 | 125.9 | 31.48 |
| 5 | The working fluid exits the turbine into the recuperator | 133.3 | 60.88 | 6.33 |
| 6 | The working fluid enters the condenser | 133.3 | 51.5 | 6.33 |
| 7 | The working fluid exits the condenser | 133.3 | 44.56 | 6.33 |
| 8 | Cooling water enters the condenser | 991.8 | 27 | 1.013 |
| 9 | Cooling water comes out of the condenser | 991.8 | 37 | 1.013 |

**Table 6**
The mass, energy, and exergy balance of the Kalina cycle.

| Component | Mass Balance | Energy Balance | Exergy Balance |
|---|---|---|---|
| Evaporator 1 | $\dot{m}_2 = \dot{m}_3,\ \dot{m}_b = \dot{m}_c$ | $\dot{m}_g(h_b - h_c) = \dot{m}_{wf}(h_1 - h_2)$ | $\dot{m}_b e_b + \dot{m}_1 e_1 = \dot{m}_c e_c + \dot{m}_2 e_2 + I_{Evaporator\ 1}$ |
| Evaporator 2 | $\dot{m}_3 = \dot{m}_4,\ \dot{m}_a = \dot{m}_b$ | $\dot{m}_g(h_a - h_b) = \dot{m}_{wf}(h_2 - h_3)$ | $\dot{m}_a e_a + \dot{m}_2 e_2 = \dot{m}_b e_b + \dot{m}_3 e_3 + I_{Evaporator\ 2}$ |
| Turbine | $\dot{m}_3 = \dot{m}_4$ | $\dot{m}_3 h_3 = W_T + \dot{m}_4 h_4$ | $\dot{m}_3 e_3 = W_T + \dot{m}_4 e_4 + I_{Turbine}$ |
| Condenser | $\dot{m}_5 = \dot{m}_6,\ \dot{m}_8 = \dot{m}_9$ | $\dot{m}_{wf}(h_5 - h_6) = \dot{m}_{ap}(h_9 - h_8)$ | $\dot{m}_5 e_5 + \dot{m}_9 e_9 = \dot{m}_6 e_6 + \dot{m}_8 e_8 + I_{Condenser}$ |
| Pump | $\dot{m}_6 = \dot{m}_7$ | $\dot{m}_7 h_7 = W_P + \dot{m}_6 h_6$ | $\dot{m}_7 e_7 = W_P + \dot{m}_6 e_6 - I_{Pump}$ |
| Recuperator | $\dot{m}_4 = \dot{m}_5,\ \dot{m}_1 = \dot{m}_7$ | $\dot{m}_4 h_4 + \dot{m}_7 h_7 = \dot{m}_5 h_5 + \dot{m}_1 h_1$ | $\dot{m}_4 e_4 + \dot{m}_7 e_7 = \dot{m}_5 e_5 + \dot{m}_1 e_1 + I_{Recuperator}$ |

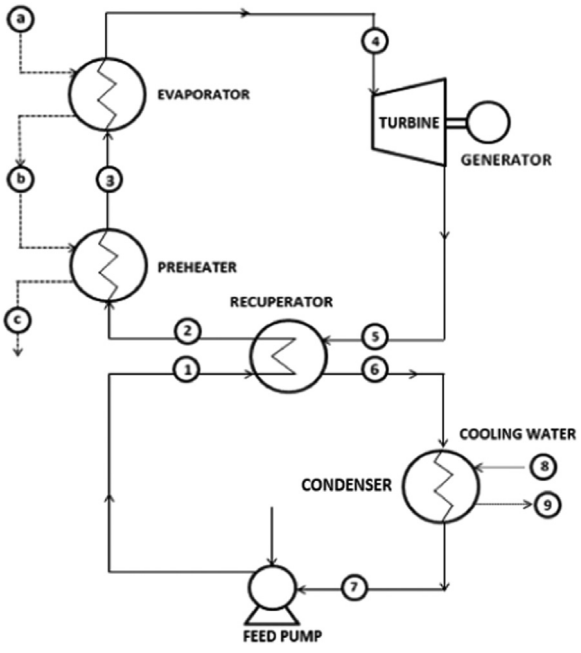


**Fig. 2.** Schematic diagram of the designed binary cycle.

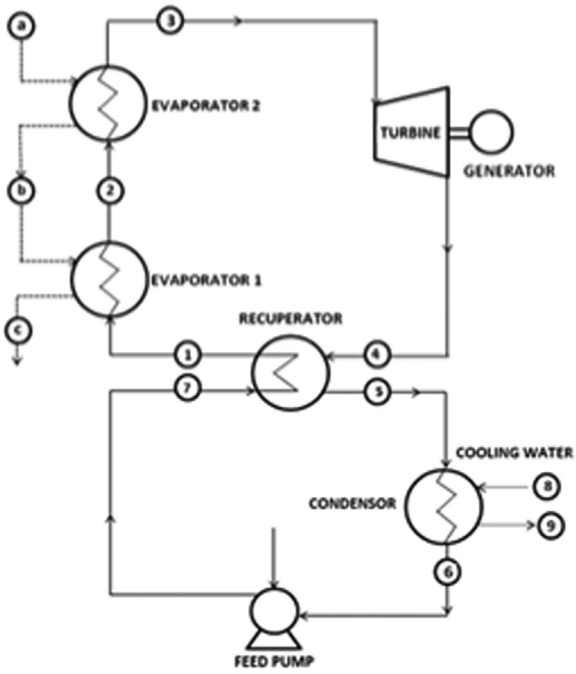


**Fig. 3.** Schematic diagram of the designed Kalina cycle.

observed in the working fluid used, as it employs a mixture of Ammonia-Water [21], and the fraction was assumed to be 84%. The mass, energy, and exergy balance equations used in the Aspen HYSYS® simulation report are shown in Table 6. After designing the model and computing the data and assumptions, the parameters obtained are presented in Table 7.

## Energy and Exergy Analysis

The first step in analyzing energy and exergy was to calculate the enthalpy (h) and entropy (s) in each condition, based on temperature and pressure, using a Computer Aided Thermodynamic Table (CATT) and Reference Fluid Thermodynamic and Transport Properties (REFPROP). Furthermore, during the steam evaluation, non-condensable gas (NCG) content was taken into account in Eqs. (3) and (4), assuming it consists of 100% $CO_2$.

$$h_n = h_{s,n}(1 - N) + h_{NCG,n}N \tag{3}$$

$$s_n = s_{s,n}(1 - N) + s_{NCG,2}N \tag{4}$$

Where $h_{s,n}$ declares the enthalpy (kJ/kg) and $s_{s,n}$ illustrates the entropy (kJ/kg.K) of steam, in n condition, whereas $h_{NCG,n}$ and $s_{NCG,2}$, states the enthalpy (kJ/kg) and entropy (kJ/kg. K) of NCG, respectively, and N is a representation of its content on a mass basis [22].

The energy analysis shows the total power, obtained by the calculation of power generated by the turbine, multiplied by its efficiency

**Table 7**
The state of each condition in the Kalina cycle.

| Condition | Information | ṁ (kg/s) | T (°C) | P (bar) |
|---|---|---|---|---|
| a | Geothermal fluid enters evaporator 2 | 27 | 160 | 6.175 |
| b | Geothermal fluid enters evaporator 1 | 27 | 160 | 6.175 |
| c | Geothermal fluid exits evaporator 1 | 27 | 93.02 | 6.175 |
| 1 | The working fluid enters the evaporator 1 | 60 | 84.05 | 31 |
| 2 | The working fluid enters the evaporator 2 | 60 | 105.4 | 31 |
| 3 | Saturated vapor working fluids enter turbines | 60 | 158.3 | 31 |
| 4 | The working fluid exits the turbine into the recuperator | 60 | 109.5 | 9 |
| 5 | The working fluid enters the condenser | 60 | 49.01 | 9 |
| 6 | The working fluid exits the condenser | 60 | 27.92 | 9 |
| 7 | Working fluid presses into the recuperator | 60 | 28.51 | 31 |
| 8 | Cooling water enters the condenser | 842.5 | 27 | 1.013 |
| 9 | Cooling water comes out of the condenser | 842.5 | 41.39 | 1.013 |

**Table 8**
Recapitulation of power calculations and efficiency of three geothermal power plant.

| Cycle | Turbine power ($W_t$) kW | Generator Power ($W_{gen}$) kW | Parasitic Load kW | Total power ($W_{gen}$) kW | Energy Efficiency % | Exergy Efficiency % |
|---|---|---|---|---|---|---|
| Dry-steam | 13,529 | 12,852 | 332 | 12,520 | 16.86 | 58.95 |
| Kalina | 9,438 | 8,966 | 1154 | 7,811 | 10.49 | 36.98 |
| Binary | 5,310 | 5,045 | 1103 | 3,942 | 5.3 | 18.66 |

and that of the generator, which was further reduced by parasitic load or the power consumed by the supporting components, as shown in Eq. (5) follows:

$$W_{total} = \left[\dot{m}\left(h_{out,turbin} - - h_{in,turbin}\right) x\ \eta_{turbin}\ x\ \eta_{generator}\right] - W_{parasitic\ load} \quad (5)$$

In calculating the exergy analysis, its balance was carried out in Eq. (4), stating that a change equivalent to the total, is transferred through the system boundary and that which was destroyed in the unit due to their irreversibility [23]. $\dot{E}$ described the exergy flow (kJ) as shown in Eq. (6), while e described the specific exergy (kJ/kg) obtained by Eq. (7).

$$< ct > \dot{E} < ot >_{in} - < ct > \dot{E} < ot >_{out} - < ct > \dot{E} < ot >_{destroyed} = \Delta < ct > \dot{E} < ot >_{sistem} \quad (6)$$

$$e = h_1 - h_0 - T_o(s_1 - s_0) \quad (7)$$

The exergy destruction $< ct > \dot{E} < ot >_D$ in the components can be compared with its rate in the whole system $< ct > \dot{E} < ot >_{in,tot}$, this comparison is called as destruction ratio $y_D$ in Eq. (8):

$$y_D = \frac{< ct > \dot{E} < ot >_D}{< ct > \dot{E} < ot >_{in,tot}} \quad (8)$$

The exergetic efficiency is defined as the ratio between the quantities of an exergy product, based on the balance in the rate of a system, as stated in Eq. (9):

$$\eta = \frac{\sum_{out}^{<ct>\dot{E}<ot>}}{\sum_{in}^{<ct>\dot{E}<ot>}} \quad (9)$$

## Results and Discussion

Based on the data obtained, the net power ($W_{net}$) can be calculated from each cycle of the turbine power and parasitic load originating from the supporting components of a generator. Meanwhile, the efficiency of the vent steam was obtained through the comparison of $W_{net}$ with the energy and exergy value, as seen in Table 8.

Table 8 shows that the dry-steam cycle could convert the highest energy among the three sequences designed. In this case, excess steam enters the cycle through the demister component, which is then directly used to turn the turbine. With the turbine output condition set to vacuum, it is possible to obtain a large specific enthalpy and exergy difference in the turbine and produce high power. Furthermore, this high turbine power was caused by a simpler design with minimal exergy elimination and reduced parasitic load, comparatively, as listed in Table 9.

**Table 9**
The composition of parasitic load for each cycle.

| Parasitic load | Dry-steam Cycle | Binary Cycle | Kalina Cycle |
|---|---|---|---|
| Pump Power | 0 kW | 731.48 kW | 795 kW |
| MCWP Power | 206 kW | 208.78 kW | 193.88 kW |
| LRVP power | 39.05 kW | 0 kW | 0 kW |
| Fan Power | 123 kW | 114 kW | 116 kW |

A comparison with the current dry-steam cycle at the existing Geothermal Power Plant showed the energy efficiency designed to have the same level, within the range of 16-17%, and the venting process of steam was attributed to low efficiency. Hence, the steam supplied is incapable of being fully utilized due to the fluctuations in pressure and excess steam occurring. In addition, the dry vapor series involved implementing as many zero venting systems as possible. Regarding parasitic load, the dry-steam cycle only consumes 332 kW or 2.65% of the power generated. This value is very different from the other two cycles because the dry-steam cycle does not require a feed pump or pump to increase the working fluid pressure until it reaches the desired Turbine Inlet Pressure as in the binary and Kalina cycles.

Table 10 describes the amount of exergy that enters, leaves, and is destroyed in the dry-steam cycle component. After passing through the demister component, dry-steam enters the turbine with an exergy of 20,987.51 kW. It undergoes an expansion process with two outputs in the form of a turbine power of 13,529 kW and the remaining steam to be condensed at 5635 kW. The turbines are the elements with the highest exergy destruction in this sequence as they are influenced by the design and construction, including flow transitions between levels, leakage around the blade tip and seal, and the final blade length. In addition, the pressure in the condenser component (vacuum) enhanced the likelihood of outside air leakages due to the presence of cracks in the expansion joint, which is estimated to increase the condenser load.

The red line in Fig. 4 describes an inverse correlation between the pressure of the condenser and turbine power. An increase in pressure

**Table 10**
Calculation results of dry-steam cycle exergy.

| Component | Exergy enter kW | Exergy out kW | Exergy wasted kW | Irreversibility kW | Irreversibility ratio % |
|---|---|---|---|---|---|
| Demister | 21239.82 | 20987.51 | 10.03 | 242.28 | 1.14 |
| Turbine | 20987.51 | 18957.61 | | 2029.90 | 9.67 |
| Condenser | 5635.01 | 3624.82 | | 2010.19 | 35.67 |

**Table 11**
Calculation results of binary cycles exergy.

| Component | Exergy enter kW | Exergy out kW | Exergy wasted kW | Irreversibility kW | Irreversibility ratio % |
|---|---|---|---|---|---|
| Evaporator | 35120.46 | 34003.97 | | 1116.49 | 3.18 |
| Preheater | 23628.83 | 13999.17 | 5596.02 | 4033.64 | 17.07 |
| Turbine | 18384.74 | 10977.39 | | 2096.676 | 11.40 |
| Condenser | 11061.01 | 7186.203 | 1984.889 | 1889.918 | 17.09 |
| Pump | 8332.183 | 7186.203 | | 1145.98 | 13.75 |
| Recuperator | 18724.38 | 18713.05 | | 11,3305 | 0.06 |

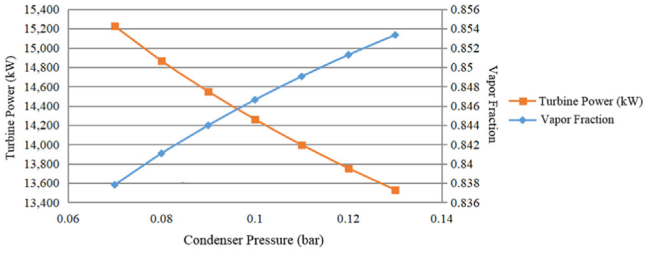


**Fig. 4.** Effect of condenser pressure on turbine power.

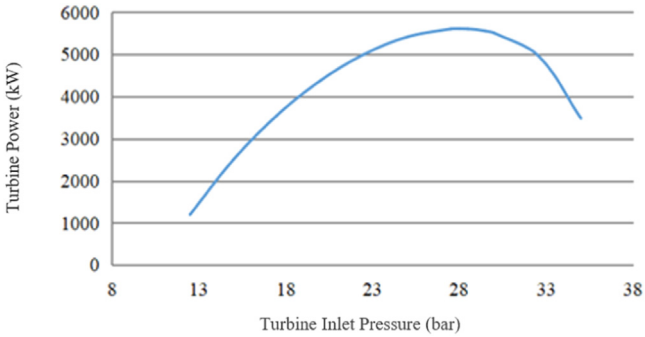


**Fig. 5.** Relationship between turbine inlet pressure (TIP) and turbine power.

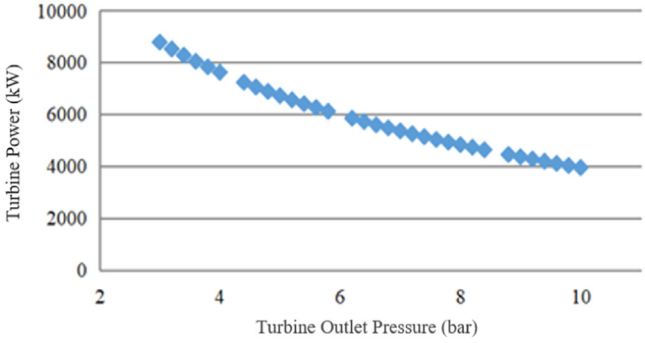


**Fig. 6.** Relationship between turbine exit pressure and turbine power.

in a specific state will cause an increase in the enthalpy and entropy values of these conditions so that the difference between the exergy entering and leaving the turbine components will be smaller and reduce the turbine power. However, the blue line illustrates the vapor fraction of steam in the varied condenser pressure, which indicates an entirely different tendency, as the decline further reduced the steam output of the turbine. However, it does not directly impact the power produced. A lower mass fraction of the vapor is related to the elevation in the liquid phase at the output, which further causes erosion within, after the cycle operates for a long time. In this case, the possible condenser pressure under actual conditions and following environmental conditions at the Kamojang geothermal power plant ranges from 0.1 to 0.13 bar. Based on these several possibilities, the optimal condition was chosen, which produces the highest turbine power and a fairly high steam fraction in the achievable range, namely at 0.1 bar condenser pressure, producing a net power of 13,160 kW.

In the binary cycle, the exergy that enters the evaporator component is 35,120 kW which comes from excess steam exergy of 21,121 kW, and exergy of Isobutane, which has been preheated by the preheater until it reaches a saturated liquid state of 13,999 kW. In the evaporator, Isobutane does not increase in temperature. It changes in phase from liquid to saturated vapor and produces an exergy annihilation value of about 1116.49 kW. The exergy of the geothermal steam coming out of the evaporator is then used for preheating the Isobutane in the preheater from a temperature of 54°C to 125.9°C. The irreversibility in the preheater components was highest among other components, as shown in Table 11. This is probably caused by several reasons, including the variation in temperature between the hot and cold fluid, the friction observed during a pass through the tube, and heat dissipation to the environment. In terms of the amount of power produced, the binary cycle is far behind the dry-steam variety. Therefore, several steps are taken to optimize the cycle, including variations in the turbine inlet pressure (TIP), with the results plotted in Fig. 5.

In Fig. 5, an increase in turbine power was observed in the TIP, from 13 to 31 bars, which became smaller through the exhibition of a decreasing line. This can, however, be analyzed from the properties of Isobutane enthalpy and entropy that are unstable near the critical pressure. Hence, the optimal TIP was obtained as 31 bars.

Conversely, optimization is also conducted with variations in the exhaust turbine, known to have a fairly large exergy of 10,977.39 kW. This was carried out by varying the output pressure in the ranges of 3–10 bars, indicating that a reduced value correlates with an elevation in power produced as shown in Fig. 6.

In the Kalina cycle, the turbine is a component with the largest exergy destruction value of 2769.6 kW, as shown in Table 12. Therefore, the system needs to be optimized based on parameters with greater influence, including ammonia mass fraction, TIP, and turbine exit pressure to obtain the maximum output power and efficiency.

**Table 12**
Calculation results of Kalina cycle exergy.

| Component | Exergy enter kW | Exergy out kW | Exergy wasted kW | Irreversibility Kw | Irreversibility ratio % |
|---|---|---|---|---|---|
| Evaporator 1 | 78955.89 | 77023.83 | | 1932.06 | 2.44 |
| Evaporator 2 | 61239.63 | 57834.6 | 899.37 | 2505.66 | 4.09 |
| Turbine | 69078 | 56870.4 | | 2769.6 | 4.0 1 |
| Condenser | 49927.92 | 47244.6 | 2636.27 | 47.0545 | 0.094 |
| Pump | 48247.8 | 47244.6 | | 1003.2 | 2.08 |
| Recuperator | 104323.2 | 102918 | | 1405.2 | 1.35 |

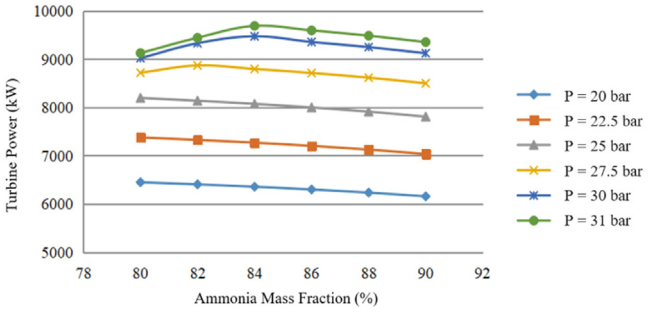


**Fig. 7.** Effect of ammonia mass fraction and TIP on turbine power.

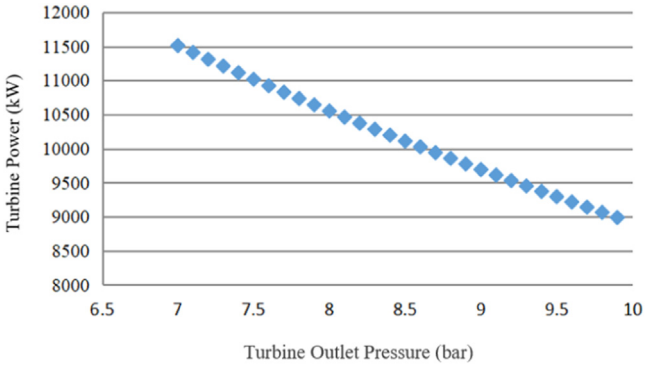


**Fig. 8.** Relationship between turbine exit pressure and turbine power.

Fig. 7 shows the effect of ammonia mass fractions, taken at intervals between 80–90% and TIP, on a scale of 20-31 bars on the turbine power. However, the difference in the amount contained in the mixture affects the temperature and the entropy value produced. Therefore, based on the graph, it can be concluded that the most optimal conditions, with the greatest yield, were observed at 31 bars, with an 84% mass fraction of ammonia.

The optimization of turbine exit pressure was in the range of 7-9.9 bars [19]. Hence, utilizing a 31 bar TIP and 84% ammonia mass fraction, the highest power was observed as 11,510 kW at the 7 bar exit pressure, as seen in Fig. 8. This increase in power will be followed by an increase in energy efficiency and generator exergy efficiency.

Optimization has been carried out from the three geothermal power plant cycles by varying parameters hypothesized to affect turbine power significantly. The results of the optimization are then summarized in Table 13.

## Economic Analysis

In determining electricity production/LEGC prices from a generator, identifying component sizing as a basis for establishing the cost of spare parts is the first step conducted. However, due to the limitations of related detailed information, the values were obtained through some literature involving a component capacity scale approach [24].

**Table 13**
Summary of the results of optimization carried out in each cycle.

| Cycle | Before Optimization | | After Optimization | |
|---|---|---|---|---|
| Dry-steam | Wt | 13,529 kW | Wt | 14,260 kW |
| | Wett | 12,512 kW | Wett | 13,160 kW |
| | Efficiency I | 16.86% | Efficiency I | 17.98% |
| | Efficiency II | 58.95% | Efficiency II | 62.83% |
| Binary | Wt | 5310 kW | Wt | 8274 kW |
| | Wett | 3942 kW | Wett | 7170 kW |
| | Efficiency I | 5.3% | Efficiency I | 9.63% |
| | Efficiency II | 18.66% | Efficiency II | 33.91% |
| Kalina | Wt | 9438 kW | Wt | 11,510 kW |
| | Wett | 7811 kW | Wett | 10,355 kW |
| | Efficiency I | 10.49% | Efficiency I | 13.91% |
| | Efficiency II | 36.98% | Efficiency II | 49.03% |

**Table 14**
Component sizing for each cycle.

| Type of Cycle | Component | Information | Value |
|---|---|---|---|
| Dry-steam Cycle | Demister | Diameter | 1.76 m |
| | Turbine | Power | 13,160 kW |
| | MCWP | Power | 186.4 kW |
| | LRVP | Capacity of NCG | 150.36 cfm |
| | Cooling tower | Air capacity | 13,800 GPM |
| | Condenser | Surface area | 5,832 $m^2$ |
| Binary Cycle | Evaporator | Surface area | 267 $m^2$ |
| | Preheater | Surface area | 513 $m^2$ |
| | Recuperator | Surface area | 447 $m^2$ |
| | Condenser | Surface area | 3,317 $m^2$ |
| | Turbine | Power | 8,274 kW |
| | Pump | Power | 731 kW |
| | MCWP | Power | 208 kW |
| | Cooling tower | Air capacity | 15,895 GPM |
| Kalina Cycle | Evaporator 1 | Surface area | 1613 $m^2$ |
| | Evaporator 2 | Surface area | 717 $m^2$ |
| | Recuperator | Surface area | 1583 $m^2$ |
| | Condenser | Surface area | 6995 $m^2$ |
| | Turbine | Power | 11,510 kW |
| | Pump | Power | 795 kW |
| | MCWP | Power | 193 kW |
| | Cooling tower | Air capacity | 13,311 GPM |

### *Component Sizing*

The component capacity determination was interpreted into several parameters according to its type, e.g., the heat exchanger. Furthermore, the value of the heat transfer surface area (A) is needed, which is known by the Log Mean Temperature Difference (LMTD) method. However, pumps and turbines require a capacity or power value [25], and the cooling tower component obliges the air capacity (calculation of cooling tower refers to the rule of thumb in wet cooling tower design [26], and the demister uses the Souders-Brown equation. Hence, the results of component sizing calculations are summarized in Table 14.

**Table 15**
The results of calculating the total capital and investment in the dry-steam cycle.

| | | | |
|---|---|---|---|
| I. Fixed capital investment | | | |
| A. Direct Cost | | | |
| 1 | Onsite Costs | | |
| | Purchased Equipment Cost | | Cost |
| | - | Demister | 19201 |
| | - | Turbine | 4330934 |
| | - | Condenser | 730367 |
| | - | Liquid Ring Vacuum Pump | 9335 |
| | - | MCWP | 65772 |
| | - | Cooling Tower | 343872 |
| | | Total purchased-equipment cost (PEC) | 5155611 |
| | Piping (10% of PEC) | | 515561 |
| | | Total Onsite Cost | 5671172 |
| 2 | Offsite Cost | | |
| | Land | | 0 |
| | | Total offsite cost | 0 |
| Total Direct Cost | | | 5671172 |
| B. Indirect Cost | | | |
| Engineering + supervision (8% of DC) | | | 453693 |
| Construction cost (15% DC) | | | 850675 |
| Contingency (20% of above the sum) | | | 260873 |
| Total Indirect Cost | | | 1565243 |
| Fixed Capital Investment (FCI) | | | 7236416 |
| II. Other Outlays | | | |
| A. Start-Up | | | 125328 |
| B. Working capital | | | 47288 |
| C. Cost of licensing, research, and development | | | 1974000 |
| D. Allowance for funds used during construction | | | 888537 |
| Total other outlays | | | 3035154 |
| Total capital investment | | | 10271570 US $ |

*Purchased Equipment Cost*

Based on the results of component sizing, it is possible to estimate purchased equipment cost (PEC) from the heat exchanger components using Eq. (10), while the power was assessed using Eq. (11) in Dorj [27]. Meanwhile, the demister and cooling tower components used the ratio method, based on the graph obtained from the chemical process design [22].

$$C_{equipment} = C_0.(size\_of\_equipment)^n \quad (10)$$

$$C_{equipment} = C_0.(power\_capacity)^n \quad (11)$$

*Total Capital Investment*

The calculation of total capital investment (TCI) uses several assumptions and methods, obtained in Dorj [27], with the results shown in Table 15, Table 16, and Table 17.

After identifying the TCI value, as well as the operating and maintenance costs from each cycle, the price of electricity production (cents/kWh) was then determined, considering economic conditions such as the fiscal age of the plant (30 years) used in Indonesia, and a Discount rate of 10%. Furthermore, the results of the LEGC were listed in Table 18, using Eq. (12) and assuming the rupiah exchange rate against the US dollar is Rp. 14,000/US $.

$$LEGC = \frac{\sum_{t=1}^{n}\left(\frac{I_t+M_t+F_t}{(1+r)^t}\right)^{-t}}{E\sum_{t=1}^{n}\frac{E_t}{(1+r)^t}} \quad (12)$$

LEGC is the cost of production per kWh (US $/kWh), $I_t$ is the total investment expenditure per year, $M_t$ is the annual operation and maintenance cost, $F_t$ depicts fuel costs, $E_t$ is the amount of electricity generated yearly, r is the discount rate, and n is the age of the generator [28].

**Table 16**
The results of calculating the total binary cycle capital investment.

| | | | |
|---|---|---|---|
| I. Fixed capital investment | | | |
| A. Direct Cost | | | |
| 1 | Onsite Costs | | |
| | Purchased Equipment Cost | | Cost |
| | - | Evaporator | 66222 |
| | - | Preheater | 111465 |
| | - | Recuperator | 197739 |
| | - | Condenser | 495502 |
| | - | Turbine | 3129704 |
| | - | Pump (feed pump + MCWP) | 332214 |
| | - | Cooling Tower | 291520 |
| | | Total Purchased-equipment cost (PEC) | 4332848 |
| | Piping (10% of PEC) | | 4332848 |
| | | Total Onsite Cost | 4766133 |
| 2 | Offsite Cost | | |
| | Land | | 0 |
| | | Total offsite cost | 0 |
| Total Direct Cost | | | 4766133 |
| B. Indirect Cost | | | |
| Engineering + supervision (8% of DC) | | | 381290 |
| Construction cost (15% DC) | | | 714920 |
| Contingency (20% of above the sum) | | | 219242 |
| Total Indirect Cost | | | 1315452 |
| Fixed Capital Investment (FCI) | | | 6081586 |
| II. Other Outlays | | | |
| A. Start-Up | | | 107857 |
| B. Working capital | | | 47288 |
| C. Cost of licensing, research, and development | | | 1241100 |
| D. Allowance for funds used during construction | | | 328862 |
| Total other outlays | | | 1725107 |
| Total capital investment | | | 7806694 US $ |

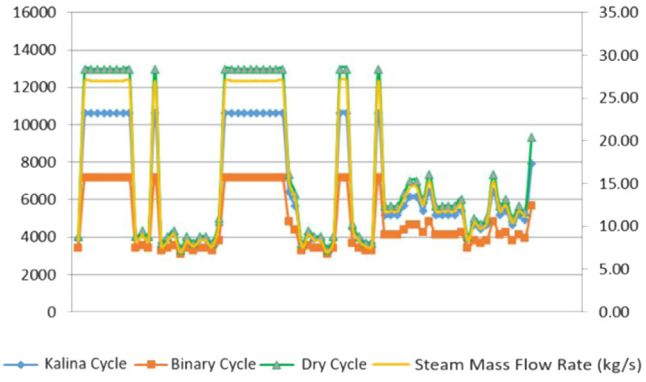


**Fig. 9.** The effect of steam mass flow to the turbine power.

*Performance Analysis*

The power plant performance is expressed by the value of the Capacity Factor (CF), which is the ratio between the actual power produced in a given period with the maximum output power of its design capacity. The value of CF is very dependent on steam mass flow (as a fuel) and the power plant design. Considering that the energy pairs or the steam used in the three cycles are the same, which has changed every time, it is necessary to analyze the effect of steam fluctuation on the output power of the three types of geothermal power plant cycles with the results described in Fig. 9.

Based on the graph obtained from the simulation of three types of geothermal power plant cycles for three days, it can be seen that the three cycles experienced fluctuations in turbine power which were influenced by changes in the mass flow rate of steam. In the dry-steam cycle design, it is due to the direct use of steam to turn the turbine. As for the binary cycle and the Kalina cycle, steam is used to heat the working fluid Isobutane or the Ammonia-Air mixture through a heat exchanger, which has a fixed capacity with a pinch point according to

**Table 17**
The calculated results of the total capital investment of the Kalina cycle.

| | | |
|---|---|---|
| I. Fixed capital investment | | |
| A. Direct Cost | | |
| 1 | Onsite Costs | |
| | Purchased Equipment Cost | Cost |
| | - Evaporator 1 | 278421 |
| | - Evaporator 2 | 145662 |
| | - Recuperator | 274317 |
| | - Condenser | 900307 |
| | - Turbine | 3066893 |
| | - Pump | 349371 |
| | - Cooling Tower | 342280 |
| | Total Purchased-equipment cost (PEC) | 5357255 |
| | Piping (10% of PEC) | 535725 |
| | Total Onsite Cost | 5892980 |
| 2 | Offsite Cost | |
| | Land | 0 |
| | Total offsite cost | 0 |
| Total Direct Cost | | 5892980 |
| B. Indirect Cost | | |
| Engineering + supervision (8% of DC) | | 471438 |
| Construction cost (15% DC) | | 883947 |
| Contingency (20% of above the sum) | | 271077 |
| Total Indirect Cost | | 1626462 |
| Fixed Capital Investment (FCI) | | 7519443 |
| II. Other Outlays | | |
| A. Start-Up | | 155110 |
| B. Working capital | | 47288 |
| A. Cost of licensing, research, and development | | 1726500 |
| B. Allowance for funds used during construction | | 598583 |
| Total other outlays | | 2325083 |
| Total capital investment | | 9844526 US $ |

**Table 18**
Prices for electricity production from three geothermal power plant cycles.

| Geothermal Power Plant | Levelized Electricity Generating Cost (LEGC) | |
|---|---|---|
| Dry-steam Cycle | 7.48 ¢ US $/kWh | IDR 1048/kWh |
| Kalina Cycle | 9.30 ¢ US $/kWh | IDR 1303/kWh |
| Binary Cycle | 11.51 ¢ US $/kWh | IDR 1612/kWh |

**Table 19**
Capacity factor (CF) of three different cycle.

| Cycle | Dry-Steam | Binary | Kalina |
|---|---|---|---|
| Capacity Factor | 57,07% | 67,33% | 60,79% |

the initial design conditions. In both cycles, the power generated also follows the mass flow rate of the steam supply in the heat exchanger because the smaller the steam mass flow rate, the lower the temperature reached by the working fluid to rotate the turbine.

Geothermal power plants generally serve as a base load, hence the need to design a new geothermal power plant cycle for a constant operation to attain maximum capacity. The power plant performance is then represented by the CF value, which is also considered in subsequent economic analyses. The Capacity Factor value can be calculated using the Eq. (13) with the result in Table 19.

$$CF = \frac{Total\ amount\ of\ energy\ produced\ during\ period\ of\ time}{Amount\ energy\ produced\ at\ full\ capacity} \quad (13)$$

*Environment Impact Analysis*

As a form of renewable energy, geothermal is a potential environmental pollutant obtained from substances within the earth and mobilized by steam to the surface, despite the smaller percentage. Steam from geothermal fields contains non-condensable gas dominated by $CO_2$ of 95–98% and $H_2S$ of 2-3%.

**Table 20**
The emissions of $CO_2$ and $H_2S$ in three cycles.

| Cycle | Capacity (MW) | Emissions (gr/kWh) $CO_2$ | $H_2S$ |
|---|---|---|---|
| Dry-Steam | 13.4 | 34.64 | 0.069 |
| Binary | 6.7 | 0 | 0 |
| Kalina | 9.94 | 0 | 0 |

Calculations of $CO_2$ and $H_2S$ emissions used in this study adopted the method of K.K. Bloomfield and J.N Moore in Yuniarto [29]. With an estimated NCG content in geothermal steam of 0.5% consisting of 99.8% CO2 and H2S of 2%, the results of the calculation of emissions released for each cycle can be seen in Table 20.

The gas removal system at dry-steam cycle possibly released 8.088,98 Ton/year of $CO_2$ and 16,18 Ton/years $H_2S$ to the atmosphere where the other system, binary and Kalina cycle, bring the gas for reinjection system to the earth. This is due to the dry-steam cycle technology, the steam that has been used to rotate the turbine and then enters the condenser still contains NCG, which is then sucked in by the LRVP. In the LRVP, NCG mixes with the service liquid and will be separated by a separator where the NCG is discharged directly into the air while the service liquid returns to the condenser.

Global warming is a current concern for most countries, including Indonesia. Indonesia is committed to reducing emissions by 29% (834 million tons of $CO_2$) by 2030. Thus, a special policy is needed to control the amount of carbon emissions in the atmosphere and to serve as an incentive approach in the form of a special levy, e.g., a tax, imposed by the government for every ton of $CO_2$ emission released.

Many countries in the world have implemented this policy which is commonly referred to as Carbon Tax. Taxes imposed by the government will motivate industry/emitters to reduce CO2 emissions if the costs they incur are less than having to pay enormous taxes each year. Several countries in Europe and Australia have implemented a carbon tax of 20 US$/ton of $CO_2$. If the carbon tax scenario is applied in Indonesia, with emissions emitted by the dry-steam cycle of 8088.98 tons, the tax to be paid will be 161,780 US$/year or more than Rp 2.26 billion/year.

*Assessment and Comparison of Three Different cycles*

Various analyses have been carried out on the three designed cycles: thermodynamics, plant performance, economic, and environmental impact. In this section, an assessment will be conducted with parameters including energy efficiency, exergy efficiency, exergy destruction, capacity factor (CF), capital costs, generated electricity costs, and environmental impacts, summarized in Table 21.

In terms of the generator's thermodynamic efficiency and the generator economics, the dry-steam cycle is superior to the other two cycles. Still, it has a weakness in the performance of the generator, namely the value of the capacity factor due to large power fluctuations. In addition, this cycle is also the only cycle that has an environmental impact by emitting CO2 and H2S emissions.

While the Kalina cycle is the second option in selecting the right cycle for the utilization of excess steam, the use of ammonia as a working fluid is currently avoided due to its high toxicity. In addition, this cycle also does not have any environmental impact similar to the binary cycle. While the binary cycle has a weakness in cycle efficiency, the capacity factor value is the best among the other two cycles even though its application is less profitable from an economic point of view due to expensive component prices and low power generated.

## Conclusion

Based on the data and analysis conducted in this study, conclusions can be drawn as described below:

**Table 21**
Assessment of three geothermal cycles from some parameters.

| Quality | Energy and Exergy Efficiencies | Exergy Destruction | Capacity Factor | Capital Cost | LEGC | Environmental Impact |
|---|---|---|---|---|---|---|
| 3 | Dry-Steam | Dry-Steam | Binary | Dry-Steam | Dry-Steam | Binary |
| 2 | Kalina | Kalina | Kalina | Kalina | Kalina | Kalina |
| 1 | Binary | Binary | Dry-Steam | Binary | Binary | Dry-Steam |
| Geothermal Cycles | Dry-Steam Cycle | Binary Cycle | Kalina Cycle | | | |
| Value | 15 | 10 | 13 | | | |

- The thermodynamic analysis was carried out in three different cycles. The dry-steam cycle generates total power ($W_{net}$) of 12,520 kW, while the energy and exergy efficiency reached 16.86% and 58.95%, respectively, with the turbine as the largest source of irreversibility at 2029 kW. Kalina cycle generates less power of 7.811 kW, with energy and exergy efficiency of 10.49% and 36.98%, respectively. Turbine and evaporator 2 are the main sources of exergy destruction. The binary cycle produces the smallest power of 3942 kW, while its energy and exergy efficiencies reached 5.3% and 18.66%, respectively. The preheater is the component with the largest irreversibility, by 4033 kW.
- Optimization was conducted to elevate the total power obtained. Meanwhile, lower condenser pressure indicates the possible production of higher turbine power using the dry-steam cycle. However, this was carried out in the binary variety with variations in the turbine inlet and exit pressure, with the ideal conditions of 31 and 3.4 bars. Furthermore, the optimization results showed an increase in the total power of 7170 kW while in the Kalina cycle. This was carried out by varying the concentration of Ammonia-Water, which increased turbine power by 24%.
- The economic analysis was conducted by calculating each cycle's total capital cost (TCC) and Levelized Electricity Generating Cost (LEGC). Therefore, the construction of a geothermal power plant with a dry-steam cycle requires an investment value of 10,271,570 US $, while that of binary and Kalina cycles were 7,806,694 US $ and 9,844,526 US $, respectively. Furthermore, the lowest production price observed in the dry-steam version was 7.48 ¢ US $/kWh, while the others were 9.30 ¢ US $/kWh and 11.51 ¢ US $/kWh, respectively.
- The performance of each cycle is evaluated by the value of capacity factor (CF) with the results of the Kalina cycle of 60.79%, the binary cycle of 67.33%, and the dry-steam cycle of 57.07%
- Environmental analysis is done by evaluating $CO_2$ and $H_2S$ emissions released into the air. The dry-steam cycle releases 34.64 g/kWh CO2 and 0.069 g/kWh H2S into the air, while the other two cycles produce zero emissions.
- The results showed the advantages of the dry-steam cycle, both in terms of energy efficiency and plant economics. Whereas the Kalina cycle and binary cycle have the advantage of minimum environmental impact by not releasing emissions into the air.

## Data availability

Visible in ALL reading formats

## Declaration of Competing Interest

The authors declare that they have no known competing financial interests or personal relationships that could have appeared to influence the work reported in this paper.

## Acknowledgment

This research was supported by Indonesia Endowment Fund for Education (LPDP), the Indonesian Ministry of Finance. We thank our colleagues from PT. Indonesia Power UPJP Kamojang who provided insight and expertise that greatly assisted the research.

## References

[1] B. Rudiyanto, M. Aries, N. Agung, W. Widjonarko, M. Hijriawan, An update of second law analysis and optimization of a single-flash geothermal power plant in Dieng, Indonesia, Geothermics 96 (March) (2021) 102212, doi:10.1016/j.geothermics.2021.102212.
[2] E. Assareh, M. Delpisheh, E. Farhadi, W. Peng, H. Moghadasi, Optimization of geothermal- and solar-driven clean electricity and hydrogen production multi-generation systems to address the energy nexus, Energy Nexus 5 (November 2021) (2022) 100043, doi:10.1016/j.nexus.2022.100043.
[3] F. Bilgili, S. Kuşkaya, P. Gençoğlu, Y. Kassouri, A.P.M. Garang, The co-movements between geothermal energy usage and $CO_2$ emissions through high and low frequency cycles, Environ. Sci. Pollut. Res. 28 (45) (2021) 63723–63738, doi:10.1007/s11356-020-11000-x.
[4] M. El Haj Assad, E. Bani-Hani, M. Khalil, Performance of geothermal power plants (single, dual, and binary) to compensate for LHC-CERN power consumption: comparative study, Geotherm. Energy 5 (1) (2017) 1–16, doi:10.1186/s40517-017-0074-z.
[5] E.E. Michaelides, Future directions and cycles for electricity production from geothermal resources, Energy Convers. Manag. 107 (2016) 186–192, doi:10.1016/j.enconman.2015.07.057.
[6] R. Bertani, Geothermal power generation in the world 2010-2014 update report, Geothermics 60 (2016) 31–43, doi:10.1016/j.geothermics.2015.11.003.
[7] R. DiPippo, Geothermal Power Plants, 2nd ed., Butterworth-Heinemann, Oxford, 2008, doi:10.1016/B978-0-7506-8620-4.X5001-1.
[8] T. Abbas, A. Ahmed Bazmi, A. Waheed Bhutto, G. Zahedi, Greener energy: issues and challenges for Pakistan-geothermal energy prospective, Renew. Sustain. Energy Rev. 31 (2014) 258–269, doi:10.1016/j.rser.2013.11.043.
[9] R. Adiprana, Evaluation and Optimization of Kamojang Unit 1-2-3 PLTP Based on Exergy Analysis, Institut Teknologi Bandung, 2014.
[10] L.A. Prananto, T.M. Fauzi Soelaiman, M. Aziz, Utilization of excess steam through dry steam cycle at Kamojang geothermal power plant, Energy Procedia 142 (2017) 160–165, doi:10.1016/j.egypro.2017.12.026.
[11] S. Suryadarma, T. Dwikorianto, A.A. Zuhro, A. Yani, Sustainable development of the Kamojang geothermal field, Geothermics 39 (4) (2010) 391–399, doi:10.1016/j.geothermics.2010.09.006.
[12] I.A. Pratama, "Design and simulation of the kalina cycle operational system capacity of 50 ton/hour using gas from the vent valve Kamojang PLTP system," Institut Teknologi Sepuluh Nopember, 2017.
[13] N.A. Pambudi, R. Itoi, S. Jalilinasrabady, K. Jaelani, Exergy analysis and optimization of Dieng single-Flash geothermal power plant, Energy Convers. Manag. 78 (2014) 405–411, doi:10.1016/j.enconman.2013.10.073.
[14] R. Adiprana, S. Purnomo, I.E. Lubis, Kamojang Geothermal Power Plant Unit 1-2-3 Evaluation and Optimization Based on Exergy Analysis, Proc. World Geotherm. Congr. (April) (2015) 19–25.
[15] N. Nasruddin, I. Dwi Saputra, T. Mentari, A. Bardow, O. Marcelina, S. Berlin, Exergy, exergoeconomic, and exergoenvironmental optimization of the geothermal binary cycle power plant at Ampallas, West Sulawesi, Indonesia, Therm. Sci. Eng. Prog. 19 (June) (2020) 100625, doi:10.1016/j.tsep.2020.100625.
[16] M.H. Seyyedvalilu, V. Zare, F. Mohammadkhani, Comparative thermoeconomic analysis of trigeneration systems based on absorption heat transformers for utilizing low-temperature geothermal energy, Energy 224 (2021) 120175, doi:10.1016/j.energy.2021.120175.
[17] D. Bharatan, E. Hoo, D. Paul, An assessment of the use of direct contact condensers with wet cooling systems for utility steam power plants, United States (1992) [Online]Available, doi:10.1016/B978-1-4160-4389-8.50098-4.
[18] R. DiPippo, Geothermal Power Plants: Principles, Applications, Case Studies and Environmental Impact, 4th ed., Elsevier Ltd., United Kingdom, 2015, doi:10.1016/C2014-0-02885-7.
[19] N. Laksminingpuri, A. Martinus, Study of the content and temperature of geothermal gas Kamojang with a grid diagram, J. Beta Gamma Isot. Radiat. Appl. 4 (2) (2013) 69–79.
[20] N.A. Pambudi, R. Itoi, S. Jalilinasrabady, K. Jaelani, Performance improvement of single-flash geothermal power plant applying three cases development scenarios using thermodynamic methods performance improvement of single-flash geothermal power plant applying three cases development scenarios using thermodyn, in: Proceedings of the World Geothermal Congress Melbourne, Aust, 2015 19-25 April 2015.
[21] A.I. Kalina, H.M. Leibowitz, Application of the Kalina cycle technology to the geothermal power generation, Geotherm. Resour. Counc. Trans. 13 (1989) 35–38.

[22] R. Adiprana, D.S. Purnomo, I.E. Lubis, Kamojang geothermal power plant unit 1-2-3 evaluation and optimization based on exergy analysis, in: Proceedings of the World Geothermal Congress Melbourne, Aust, 2015 19-25 April 2015.
[23] A. Bejan, G. Tsatsaronis, M. Moran, Thermal Design and Optimization, John Wiley & Sons, Inc, New York, 1996.
[24] H.P. Loh, J. Lyons, and C.W. White, "Process equipment cost estimation final report," United States, 2002. doi: 10.2172/797810.
[25] A. Mereto, M.S. Guðjónsdóttir, V. Chauhan, Thermoeconomic Analysis of Geothermal Power Cycles for IDDP-1 Chloride Mitigation, Reykjavík University, 2016.
[26] S. Leeper, "Wet cooling towers: rule-of-thumb design and simulation," United States, 1981. doi: doi:10.2172/5281927.
[27] P. Dorj, Thermoeconomic Analysis of a New Geothermal Utilization CHP Plant, University of Iceland, 2005.
[28] U.S. Department of Energy Office of Indian Energy Policy and ProgramsLevelized Cost of Energy (LCOE), United States, 2015 [Online]. Available: https://www.energy.gov/sites/prod/files/2015/08/f25/LCOE.pdf%0Ahttps://energy.gov/sites/prod/files/2015/08/f25/LCOE.pdf .
[29] Yuniarto, T.E.B. Soesilo, E. Heviati, Geothermal power plant development in indonesia, in: Proceedings of the World Geothermal Congress, 2015, pp. 1–5.